Correlations to estimate the ground loading from small scale propane BLEVE experiments

El Mehdi Laamarti, A.M. Birk, Clément Chanut, Frederic Heymes

Process Safety and Environmental Protection 185 (2024) 876–889

Contents lists available at ScienceDirect

Process Safety and Environmental Protection

journal homepage: www.journals.elsevier.com/process-safety-and-environmental-protection

Correlations to estimate the ground loading from small scale propane BLEVE experiments

E.M. Laamarti [a,b], A.M. Birk [a], C. Chanut [b], F. Heymes [b,*]

[a] Queen's University Department of Mechanical and Materials Engineering, McLaughlin Hall, Kingston, ON K7L 3N6, Canada
[b] Laboratoire des Sciences des Risques, IMT Mines Ales, Ales, France

ARTICLE INFO

Keywords:
Ground load force
Force duration
Impulse
Propane
Boiling liquid expanding vapor explosion
BLEVE
Crack velocity
Explosion
Safety

ABSTRACT

This paper presents small-scale propane BLEVE (Boiling Liquid Expanding Vapor Explosion) experiments coupled with an investigation into ground loading dynamics. The experiments utilized cylindrical aluminum pressure vessels, with a diameter of 50 mm and a length of 300 mm. The controlled variables included burst pressure, liquid fill level, and weakened length. Both high and low-speed measurements of internal pressure and ground force were conducted during the experiments. The dependent variables analyzed were peak total ground load, force duration, and impulse. The findings from the study show trends in ground force and impulse with alterations in failure pressure, fill level and weakened length. Specifically, ground force and impulse exhibit an upward trend with increasing failure pressure, fill level and weakened length (cut length). For the first time, comprehensive correlations have been developed, incorporating the controlled variables, as well as theoretical boiling wave speed and vapor speed, to estimate the dependent variables, which represents a significant contribution in the field. However, the study does acknowledge the presence of scatter in the data, which are believed to be associated with the intricacies of the vessel opening process. It should be noted that this correlation has not been validated for larger scales. Once validated on a larger scale, these correlations can be directly applied in the design and practice of civil infrastructure to enhance the structural integrity. Additionally, the research has direct implications for industrial applications, allowing for the quantitative assessment of risks associated with bridge collapse during the transportation of PLGs.

1. Introduction

In the worldwide industrial milieu, particularly within the chemical and energy sectors, ensuring the safe transportation and storage of hazardous materials remains a paramount concern. Indeed, a significant portion of commercial products is contained as pressure liquefied gases (PLGs), such as propane, ammonia, and hydrogen, housed in pressure vessels. Nevertheless, the integrity of these pressure vessels may be compromised by various internal and external factors, leading to the risk of a Boiling Liquid Expanding Vapor Explosion (BLEVE). Numerous BLEVE accidents transpired between 1941 and 1990, although only a limited number of them were officially documented, owing to the fortuitous occurrence of many taking place in sparsely populated regions where the impact on both human life and infrastructure remains minor. Within this context, Abbasi and Abbasi (2007) conducted an exhaustive review of BLEVE incidents.

One current definition of BLEVE was given by Birk et al. (2007), as the sudden release of energy resulting from the total loss of containment (i.e., full opening) of a pressure vessel containing a pressure-liquefied gas (PLG). This type of explosion entails an exceptionally destructive event, characterized by the generation of strong blast waves, significant thrust forces, and projectiles. The release can lead to vapor cloud explosions (VCE), fireballs and flashfire (Birk, 1996). Most studies on BLEVE have focused on fireball thermal radiation, shock overpressure and projectiles distances. Over the years, an experimental database documenting BLEVE has been established at various scales. The vast majority of existing data focuses on the far-field effect, as demonstrated in studies such as Planas-Cuchi et al. (2004), and yet the understanding of the physics is not complete. Laboureur et al. (2012) conducted small-scale supercritical BLEVE experiments (not strictly a BLEVE). Subsequently, Laboureur et al. (2015) investigated various methods for selected test series to elaborate a new modeling approach for BLEVE overpressure. Additionally, Birk et al. (2018) introduced a physical approach to the shock start that does not require evaluation of the

* Corresponding author.
E-mail address: frederic.heymes@mines-ales.fr (F. Heymes).

https://doi.org/10.1016/j.psep.2024.03.006
Received 7 January 2024; Received in revised form 26 February 2024; Accepted 3 March 2024
Available online 5 March 2024

expansion energy for predicting the near-field BLEVE overpressure. Very few studies have looked at the ground loading and so far, no correlation has been established for this hazard. Recent incidents have focused some attention on ground loading from BLEVE.

Interrogations from emergency responders regarding the repercussions of a BLEVE on civil infrastructure, such as its potential to cause bridge destruction, underscore the need of understanding these phenomena. By predicting ground load parameters in small-scale BLEVEs, the study directly addresses concerns related to public safety, particularly in scenarios involving hazardous events like tank truck accidents. Small scale-controlled experiments of propane BLEVE were started in 2015 at IMT mines Ales. These experiments introduced a blast plate under the vessel to measure ground loading during a BLEVE. This was reported by Eyssette (2018) in his PhD thesis, and by Eyssette et al. (2021). They showed very significant ground loading even in small scale. Birk et al. (2019) investigated the initial stages of small-scale BLEVE events using shadowgraph high-speed imaging. Their findings indicate that the ground loading phenomenon is primarily governed by the liquid flashing process. Furthermore, the study reveals that the magnitude of the ground force depends on factors such as the speed of vessel opening, failure pressure, tube dimensions and the liquid fill level.

Subsequently, the tragic incident in Bologna, Italy August 2018 (BBC news, 2018), cast a spotlight on the ground loading from a BLEVE. In this incident, a BLEVE occurred due to a traffic accident involving a tanker truck carrying LPG, leading to a partial bridge collapse along with fatalities and injuries. The significance of the ground load was evident and refers to the force and impulse exerted on the ground beneath the vessel during a BLEVE event. More recently in late 2022, another BLEVE occurred in Johannesburg, South Africa, (CTV news, 2022), when a tanker became lodged under the bridge, leading to a thermal induced BLEVE and to bridge partial breakdown along with casualties. These tangible incidents clearly demonstrate the importance of near-field loading such as ground loading and related vertical forces.

This paper presents a set of new ground load data from the Laamarti 2022 experimental campaign, complemented by data from Eyssette (2018). The current study aims to extend the existing data for a broader range of controlled variables (burst pressure, fill level, weakened length). The investigation combines numerical and experimental approaches to correlate, for the first time BLEVE ground load parameters with controlled variables. Validation is needed for larger scales. Successful validation could potentially help predict the ground load, improve safety measures, and reduce material and human risks associated with BLEVE incidents. Moreover, this could serve as a practical tool for civil infrastructure engineers to address the engineering challenges related to the resilience of bridges against ground forces during BLEVE event.

2. Dimensional analysis

During the 2022 BLEVE experiments, various factors had an important role in shaping the results. These factors can be categorized into independent and dependant variables. The independent variables are mostly those controlled and selected to attain the desired burst conditions. For instance, these include the following fixed conditions:

- The dimensions of the vessel including: L_v: length (0.3 m) | D: Diameter (0.05 m)
- The material composition of the vessel: Aluminum 6061 T6 annealed to T0.
- The nature of the contained substance: Propane 99.5%

Within the framework, the following variables were altered:

- The burst pressure P_f [Barg]
- The liquid fill level (volume fraction) φ
- The weakened length L_c [m]. The tubes were machined to induce a failure along the vessel top.

Variations in theses independent variables were employed to generate data for the dependant variables that included the following:

- Peak ground load force F [kN]
- Ground load duration t [ms]
- Ground load impulse I [N.s]

A dimensional analysis was employed to develop correlations capable of predicting accurately the dependant variables. In this analysis all variables are made dimensionless by appropriate dependant variables. This method simplifies the analysis and facilitates the development of correlations. The method is well described in next section.

Thus, the correlations were built based on the three independent variables listed previously. In addition, to the already dimensionless fill level φ, the burst pressure was normalized by the atmospheric pressure, as a standard reference, and the weakened length was normalized by the tube length as follows:

$$P^* = \left(\frac{P_f}{P_{atm}}\right);\ L^* = \left(\frac{L_c}{L_v}\right);\ P_{atm}: \text{Atmospheric pressure } (1.01325) \text{ [Bar]}$$

3. Dimensional dependant variables

3.1. Peak ground load force

The peak ground force can be normalized by the burst pressure times the vessel projected area. This gives the following normalized dimensionless peak ground force:

$$F^* = \frac{F}{P_f A} = \frac{F}{P_f D L_v} \tag{1}$$

Where,

F: Experimental peak ground load [kN]
A: Vessel projected surface [m^2]
F^* : Dimensionless peak ground load

3.2. Duration of ground load

The ground load duration is an important dependant variable that helps determine the ground impulse. The experimental value corresponds to the base of the triangular shaped peak ground load. The ground load duration is non-dimensionalized by dividing the duration by the sum of two theoretical durations - one for the vapor release and one for the liquid release. The ratio between the experimentally measured and the theoretically estimated durations of the vapor and liquid releases yields to the dimensionless duration. Within this study, the dimensionless ground load duration relation is:

$$t^* = \frac{t}{t_{liq} + t_{vap}} \tag{2}$$

To estimate the time of liquid and vapor releases we use simple 1D models of the release process. For the liquid we use a 1D choked boiling wave analysis. For the vapor we use a simple choked vapor flow model. In both cases we do not know the correct flow area to use so we use the product of $D.L_c$. This will be correct only for full opening of the vessel. To determine the theoretical time of the release we need to divide the known mass by the estimated mass flow rate of the release. Further details of how these various terms are calculated are given in the appendix.

3.3. Impulse

The experimental impulse is ascertained through the integration of the ground load curve over time, for the full duration of the ground load. The impulse is modeled as a triangular wave with the base being the duration of the ground load times the peak ground force divided by two.

$$I = \frac{Ft}{2} \tag{3}$$

t: Experimental duration of ground load [s]
I: Experimental Impulse [kN. s]

3.4. Correlation equations

The dependant data obtained for ground load and impulse has been correlated to the independent variables. Each non-dimensional dependant parameter (G) was correlated using the equation below. The values of the exponents a, b and c and the constant K will depend on the parameter being correlated.

$$G = K_1\left(\frac{P_f}{P_{atm}}\right)^a(\varphi)^b\left(\frac{L_c}{L_v}\right)^c$$

The dimensionless expression denoted for the peak ground force can be correlated as follows:

$$F^* = \frac{F}{P_f A} = \frac{F}{P_f D L_v} \quad F^*_{cor} = K_1\left(\frac{P_f}{P_{atm}}\right)^a(\varphi)^b\left(\frac{L_c}{L_v}\right)^c \tag{4}$$

Through this formulation, the correlated peak ground load can be described by the following equation:

$$F_{cor} = P_f D L_v K_1\left(\frac{P_f}{P_{atm}}\right)^a(\varphi)^b\left(\frac{L_c}{L_v}\right)^c \tag{5}$$

Where F_{cor} is the correlated peak ground force. [kN]

Similarly, to the peak ground load, the associated duration of the ground load corresponds to:

$$t_{cor} = K_2\left(\frac{P_f}{P_{atm}}\right)^d(\varphi)^e\left(\frac{L_c}{L_v}\right)^f(t_{liq} + t_{vap}) \tag{6}$$

Where t_{liq} is estimated from the boiling wave analysis and t_{vap} from the choked flow estimation.

The correlated impulse is then determined by the following relation which assumes a triangle shape of the ground force versus time function:

$$I_{cor} = \frac{F_{cor} t_{cor}}{2} \tag{7}$$

4. Apparatus of small scale BLEVE experiments

The small-scale BLEVE experimental setup shares similarities and incorporates updates on the one outlined by Eyssette (2018). A brief description of the apparatus is presented here.

Pure propane was introduced into the tubes, for the desired fill level (or grams of propane). Then the tube bottom, underwent gradual electrical heating until the tube experienced burst failure. To capture the transient ground load, the tube was supported on top of a blast plate (length = 400 mm and width = 100 mm) mounted on four high-speed load cells (22.1 mm diameter). The experimental instrumentation deployed the following high and low-speed instruments, including:

- Three high-speed cameras positioned for varied views:
  - ➢ Phantom V2512 (10,000 fps (frames per second) / 1280×800 pixels / exposure time: 66 μs) (Front side)
  - ➢ Phantom V711 Nikkon 70/300 mm (15,000 fps / 512×512 / exposure time: 90 μs) (Window side)
  - ➢ Photron FASTCAM SA5 Canon 100/400 mm (5000 fps/ 1024×1024 /exposure time: 200 μs). (End side)
- Thirteen pencil blast gages PCB 137A23 positioned at various orientations (horizontal/vertical/45 degrees) across different locations to measure the overpressure.
- Thermocouples type k at the middle of the tube in both liquid/vapor phases, 1 mm diameter (TC-direct 716–072).
- Low and high-speed pressure transducers at the tube end fitting, including one piezoelectric pressure sensor PCB M101A02 transducer.
- Four piezoelectric load cells PCB M202B.
- Additional equipment such as an electric heater (125 watts), electric valves for purging/venting, a propane weight scale, a tube cradle, Swagelok end fittings with ferrules, and an infrared camera FLIR GASFIND to detect leaks.

The experimental apparatus was designed to replicate a pressure vessel failure with a length-to-diameter ratio (L_v /D) of 6, and the presence of a weakened length at the top simulates a pressure vessel with top failure. The scale and low cost of the tubes made it possible for indoor experiments and the conduct of many experiments. Fig. 1 displays the developed apparatus, with one end featuring a window to allow the observation of the flashing process inside the vessel.

5. Results and discussion

5.1. Experiments overview

In 2022, a set of 36 small-scale BLEVE experiments were conducted, and aimed at expanding upon and refining the data obtained from Eyssette (2018). The results demonstrated significant improvements with more consistent outcome in controlling burst pressure. Additionally, the experimental campaign generated new data on 100% liquid fill levels and new insights into ground loading, near-field overpressure, shock formation and boiling wave characteristics over a wider range of controlled variables.

Fig. 2a) summarizes findings obtained by Eyssette (2018) and experiments carried out in 2022.The experiments conducted in 2022 were centered around investigating the effects of varying weakened lengths at different fill levels. Additionally, the study also delved into analyzing the extreme scenario of the longest weakened length in conjunction with a 100% fill level. This particular configuration was chosen to examine and comprehend the dynamics of the rupture with no vapor space.

Further details on the operating conditions and the ground load parameters from BLEVE 2022 and Eyssette (2018) BLEVE are presented in the appendix.

Fig. 2b) shows the Pressure-Temperature (PT) diagram for pure propane, showing both the saturation curve and the liquid spinodal line. Within this graphical representation, the failure pressures and temperatures from each individual test are shown. It is evident that most of the tests resulted in the vessel bursting with both liquid and vapor phases at saturation conditions. There are a few cases above the saturation line. This was because the vessel went liquid full, with the liquid in a compressed state. For those cases, the vessel went liquid full before burst, thus the pressure increase was driven by hydrostatic conditions rather than saturation conditions. In these cases, the partial rupture of the vessel would have caused a rapid drop in pressure to the saturation condition, and this would have affected how the vessel opens. As a direct outcome of these hydrostatic conditions, these vessels experienced partial failure and not full opening. This considerably reduced the blast strength and ground load compared to other tests. Hence the tests involving 100% liquid fill constitute a special case of BLEVE, showing a different behavior compared to other tests, that needs further investigation. Consequently, the correlations established in the subsequent analysis are not applicable to situations involving a full 100% liquid fill case.

5.2. Peak ground load results

Fig. 3 summarizes the results from both Eyssette (2018) and the 2022 experimental campaign. It clearly shows the contributions of failure pressure, fill level, and weakened length to the peak ground force. We see the following:

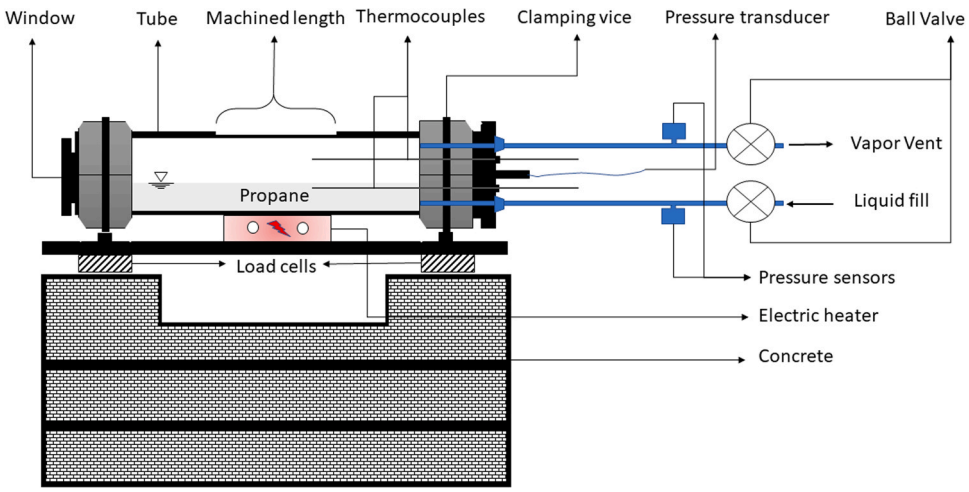

Fig. 1. Schematic Diagram of apparatus.

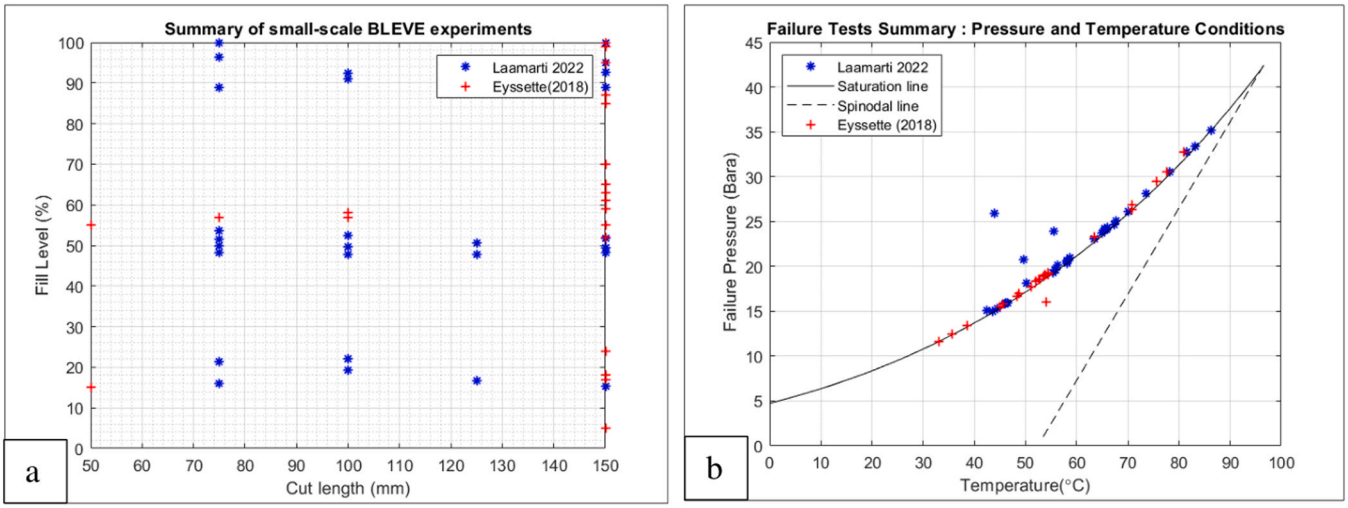

Fig. 2. Summary of BLEVE operating conditions [Laamarti 2022/ Eyssette (2018)**].**

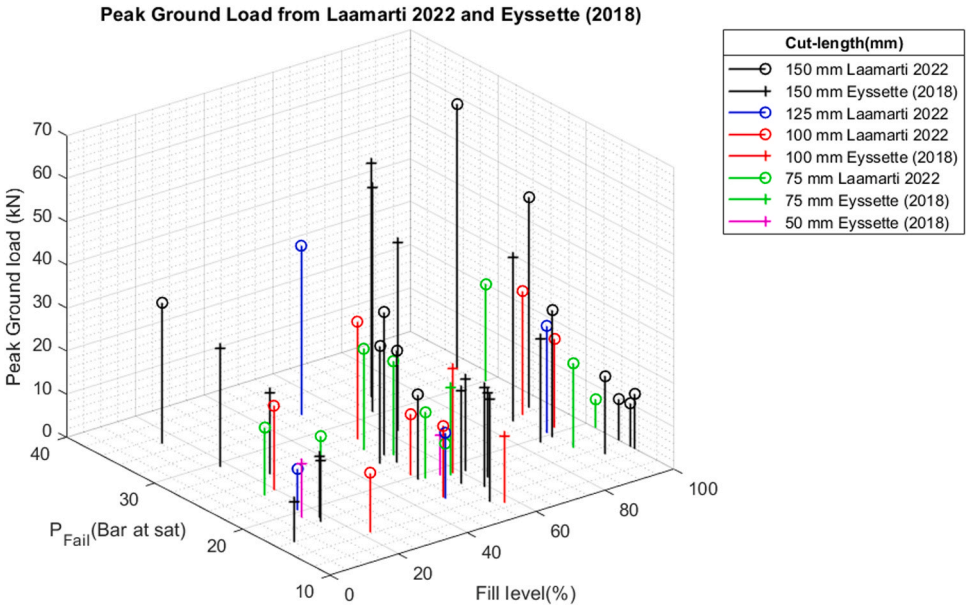

Fig. 3. 3D Plot of ground load vs failure pressures, fill levels - with cut lengths shown in symbols.

i) The highest failure pressure gave the highest peak ground force.
ii) The longest weakened length resulted in the generation of the strongest ground load.
iii) High liquid fill levels induced high ground load force. (except for 100% fill level)
iv) At lower failure pressures the liquid fill level and weakened length were not as important. This suggests the degree of superheat upon failure is important for the magnitude of the ground load.

This finding underscores the important contribution of the liquid phase superheat to the overall ground force.

By looking closely into the results, several tests can be compared, with each test varying one variable parameter at a time to examine the individual contribution. Examples of these are presented in Fig. 4. They include:

- Test 20: 20% fill, 100 mm weakened length, 24.1 Barg burst pressure.
- Test 19: 90% fill, 100 mm weakened length, 23.3 Barg burst pressure–Highest peak ground force.
- Test 25: 20% fill, 100 mm weakened length, 13.1 Barg burst pressure– Lowest peak ground force.
- Test 29: 20% fill, 75 mm weakened length, 22.4 Barg burst pressure.

Fig. 4 shows that all the tests undergo the same BLEVE steps. First, the pressure vessel attains its burst pressure and succumbs to a top failure. This event allows the vapor to leave the vessel to expand rapidly causing an initial depressurization that triggers flashing in the liquid. The flashing process causes a recovery in pressure in the vessel which drives the crack opening forward. During the pressure transient, the flashing process propagates through the superheated liquid. The resulting pressure and momentum forces cause the ground loading to grow and decay (orange curve). This triangle -shaped force reaches its maximum when the pressure vessel totally opens.

For example, in test 20, we see a peak ground force of 19.6 kN. In this test, we see a small bump in the beginning of the ground load possibly due to the vapor leaving. At the same time, the pressure is dropping in the vessel. Then we see a pressure recovery as the liquid flashes. This produces the main ground load which has a triangular shape on the Force-time plot. We see a few bumps on this triangle probably due to changes in the growth of the crack and the opening of the vessel. The actual timing and shapes of the ground load curves are contingent upon the manner in which the pressure vessel opens, particularly its crack propagation speed. This variability can introduce asymmetry into the process of the wall flaps opening, causing an uneven distribution of the ground force across various load cells and potentially lead to certain delays in the vessel opening.

By looking closely to Fig. 4, the contribution of each parameter can be determined between each test. When increasing the fill level from

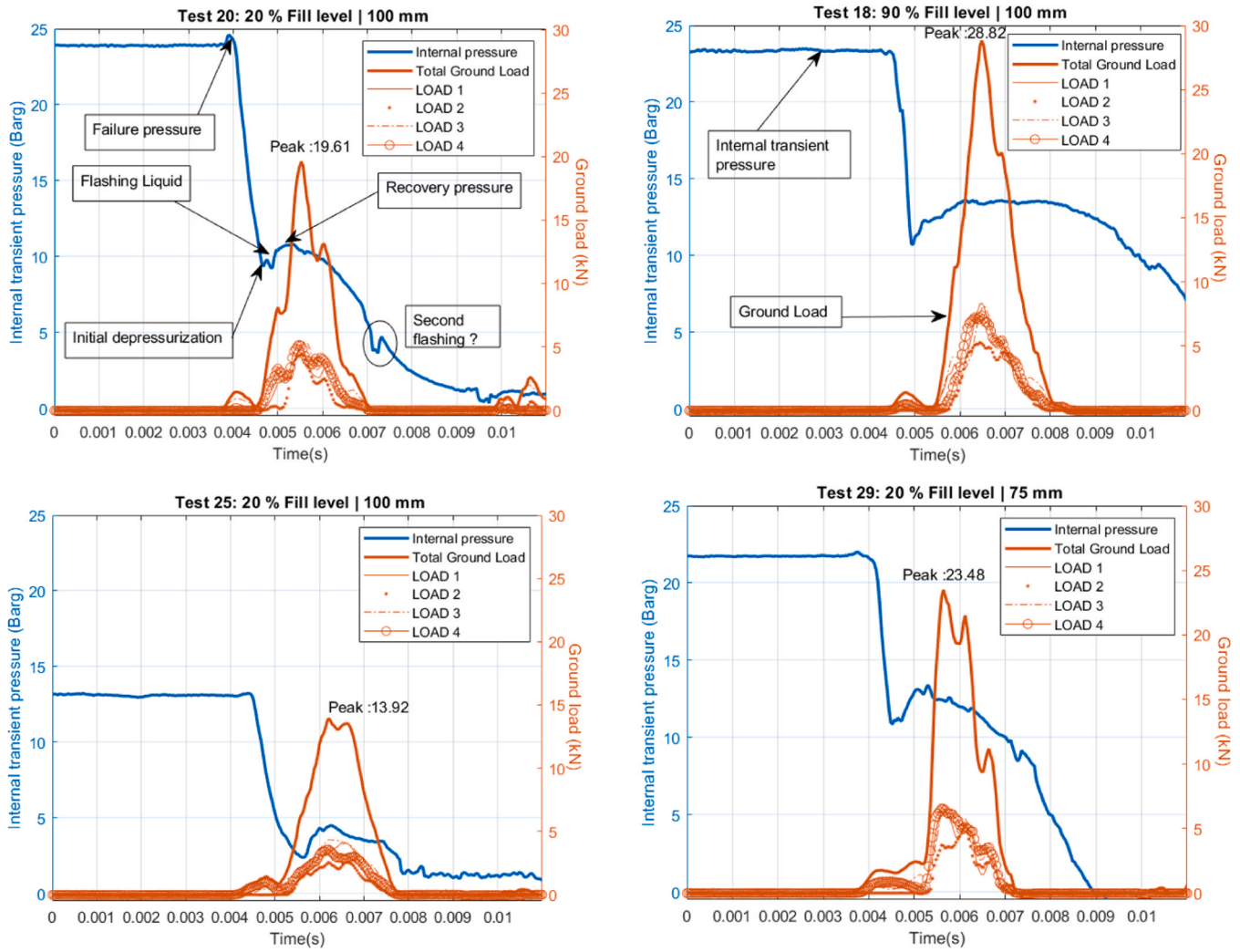

Fig. 4. Ground loading and internal pressure (Tests 18, 20,25,29) from Laamarti 2022.

20% to 90%, as seen in Test 18 compared to Test 20 under the same operating conditions, the ground load significantly increases by 35%, highlighting the liquid boiling process dominance. On the other hand, the ground load is lower when the tube bursts at lower pressure as in Test 25. Finally, the weakened length tends to increase the ground load between Test 20 and 29. Consequently, through iterative analysis, the exponents of Eq. 2 can be determined.

Correlation results

Fig. 5 shows the dimensionless ground load correlation with the optimal fit to the experimental results from 2022 campaign. Subsequently, the identical correlation was applied on data from Eyssette et al. (2021) which resulted in very consistent prediction. Nonetheless, the graph shows scattering in the data probably caused by random variables in the failure opening process. We are mostly interested in the maximum forces observed, not just the average. The obtained correlation for the dimensionless force is:

$$F^*_{cor} = 0.41\left(\frac{P_f}{P_{atm}}\right)^{0.34}(\varphi)^{0.28}\left(\frac{L_c}{L_v}\right)^{0.34} \tag{11}$$

Fig. 6 compares the experimental peak ground load with the correlated one. Ideally, the two values should be equal which would suggest a perfect correlation. The stochastic part of the vessel opening dynamics revealed some scatter in the results. Data showed that similar BLEVE conditions did not always yield the same ground load and impulse. Failures with the most rapid opening are believed to lead to stronger hazards. We will discuss this further later on. To cover the upper bounds of the cloud of data we use the formula.

$$F_{corr\_max} = kF_{cor} \quad k = 1.49 \tag{12}$$

The average correlation for peak ground load is:

$$F_{cor} = 0.41\left(\frac{P_f}{P_{atm}}\right)^{0.34}(\varphi)^{0.28}\left(\frac{L_c}{L_v}\right)^{0.34} P_f LD \tag{13}$$

5.3. Ground load duration results

The duration of the ground load is needed to determine the ground load impulse from the BLEVE. In some case scenarios, a lower ground force with a longer duration can result in a higher impulse and more damage potential. Similarly, to the previous section, the scatter in the data from the measured duration of ground load can be approximated using the correlation curve fit. Fig. 7 shows the load duration vs the failure pressure and fill level for different weakened lengths. It can be deduced that:

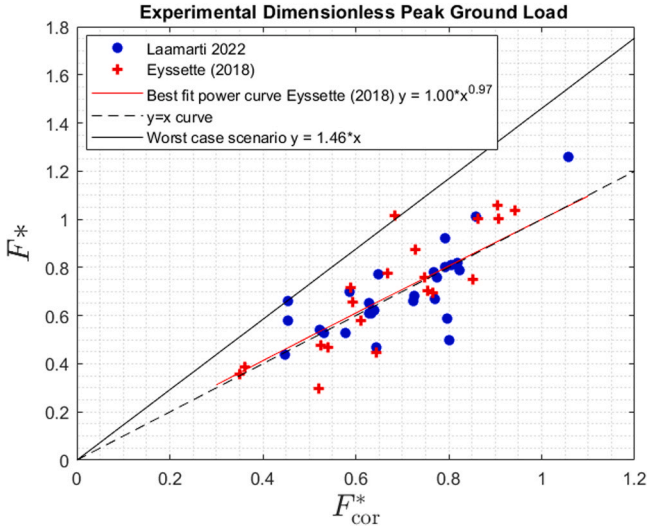

Fig. 5. Dimensionless Ground Load.

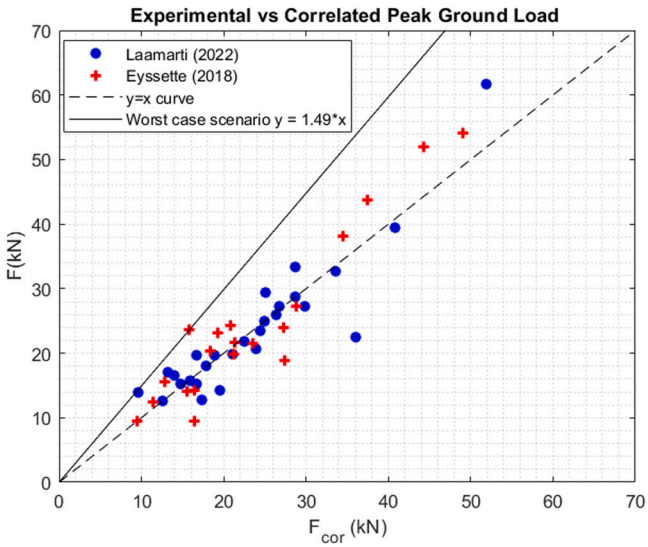

Fig. 6. Experimental vs Correlated Ground Load.

i) The duration is shorter for low liquid fill levels and higher failure pressures.
ii) Low liquid fill levels empty faster due to the high speed of sound in the vapor phase.
iii) The liquid phase takes longer to empty because of the slow boiling wave speed (low speed of sound in 2-phase mixture).

The high failure pressures led to shorter duration as more energy is available to rapidly empty the vessel's content. We expected to see shorter durations with longer weakened lengths, but this is not clear from the data.

The best fit correlation for the ground load duration is given below. Likewise, just as the maximum ground force, the duration of ground load can be also estimated as seen in Fig. 8. The obtained correlation for the dimensionless duration is:

$$t^*_{cor} = 1.44\left(\frac{P_f}{P_{atm}}\right)^{0.13}(\varphi)^{-0.61}\left(\frac{L_c}{L_v}\right)^{1.12} \tag{14}$$

The dimensionless duration is strongly affected by increases in the weakened length and the failure pressure while it is negatively impacted by increases in fill level. Fig. 8 shows the curve fit for the dimensionless duration.

Fig. 9 shows the experimental duration vs the correlated duration. There is reasonable agreement between the correlated and the experimental duration with some scatter. For most points, the correlation is good. For certain data points, the experimental duration appears to be longer than expected. Upon further examination, a partial failure was observed for these cases. Due to the small weakened length, the internal pressure was not strong enough to fully open the tube. This slower and smaller opening resulted in a slower release of the contents. This indicates the significance of the weakened length in defining the duration of the ground load.

To cover the upper bounds of the cloud of data we use the formula.

$$t_{corr\_max} = kt_{cor} \quad k = 1.61 \tag{15}$$

The correlated duration of ground load can be approximated using the following equation:

$$t_{cor} = 1.44\left(\frac{P_f}{P_{atm}}\right)^{0.13}(\varphi)^{-0.61}\left(\frac{L_c}{L_v}\right)^{1.12}(t_{liq} + t_{vap}) \tag{16}$$

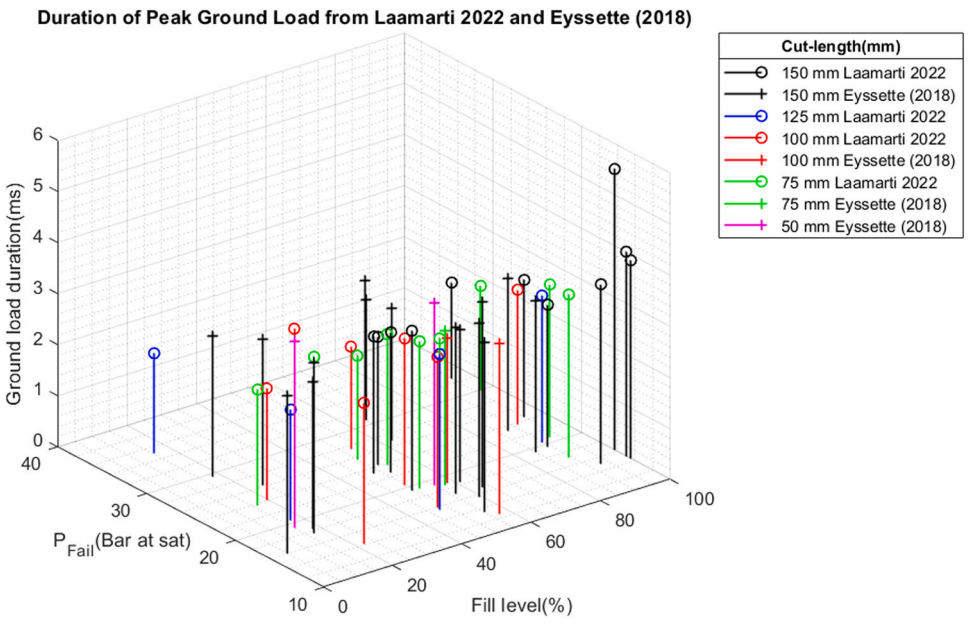

Fig. 7. 3D Plot of ground load duration vs failure pressures, fill levels - with cut lengths shown in symbols.

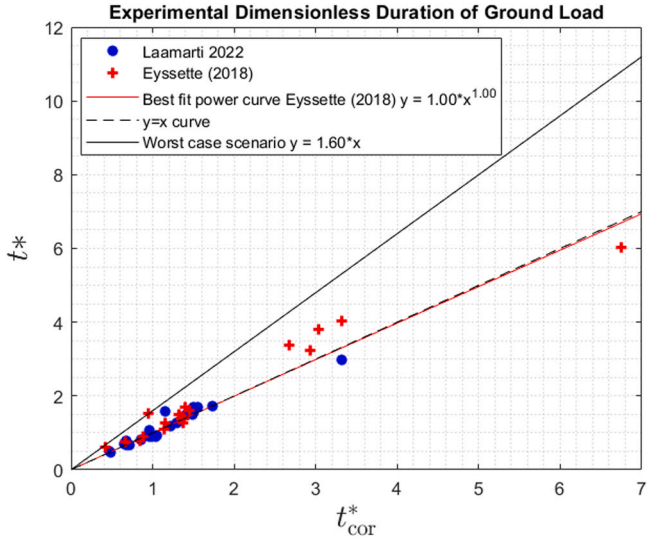

Fig. 8. Dimensionless Ground Load Duration.

5.4. Impulse results

Fig. 10 shows the experimental impulse for the diverse experimental conditions. We see the following:

i) The highest ground impulse is with high failure pressure (high superheat level), high fill level and long weakened length.
ii) Impulse increases with increased failure pressure
iii) Impulse increases with liquid fill level.
iv) Impulse increases with longer weakened length.
v) The lowest impulse is with the low failure pressure and low fill level and small weakened length.

The vapor phase has a less pronounced impact on the ground load impulse. As a result, a strong belief lies, that is in contrast with vapor phase energy, the high liquid phase thermal energy dominates the impulse. Once again, the fill level is most important at high failure pressures where liquid superheat is large. Large superheat gives strong flashing upon pressure drop.

The dimensionless impulse curve fit is shown and formulated as follows:

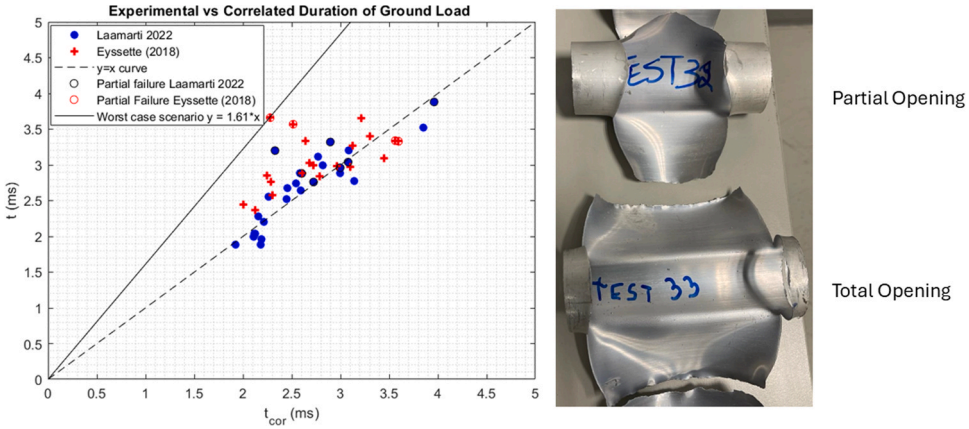

Fig. 9. Experimental vs Correlated Ground Load Duration.

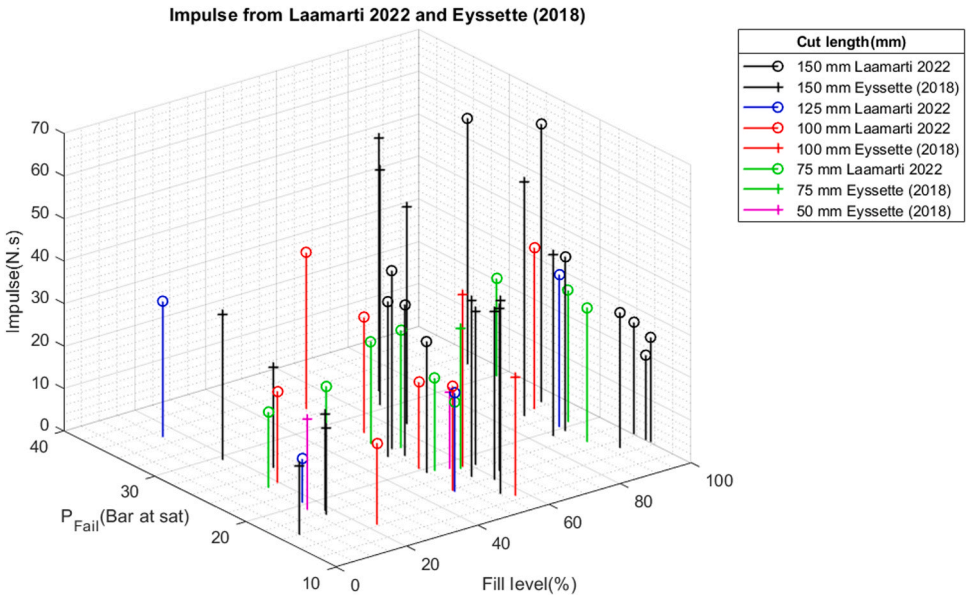

Fig. 10. 3D Plot of Impulse vs failure pressures, fill levels - with cut lengths shown in symbols.

$$I^*_{cor} = \frac{F^*_{cor} \quad t^*_{cor}}{2} = 0.29\left(\frac{P_f}{P_{atm}}\right)^{0.47}(\varphi)^{-0.33}\left(\frac{L_c}{L_v}\right)^{1.46} \tag{17}$$

Fig. 12 shows the experimental impulse vs the correlated impulse. Once again, we see reasonable agreement between the experiments and the correlation.

Similarly, to previous sections, the experimental impulse was compared to the correlated impulse. It is noteworthy that tests with partial failure were underpredicted because of the higher experimental impulse.

To estimate the most severe case of BLEVE, the following approach is suggested.

$$I_{corr\_max} = kI_{cor} \quad k = 1.67 \tag{18}$$

The average impulse equation is:

$$I_{cor} = 0.29\left(\frac{P_f}{P_{atm}}\right)^{0.47}(\varphi)^{-0.33}\left(\frac{L_c}{L_v}\right)^{1.46}\frac{P_f L_v D(t_{liq}+t_{vap})}{2} \tag{19}$$

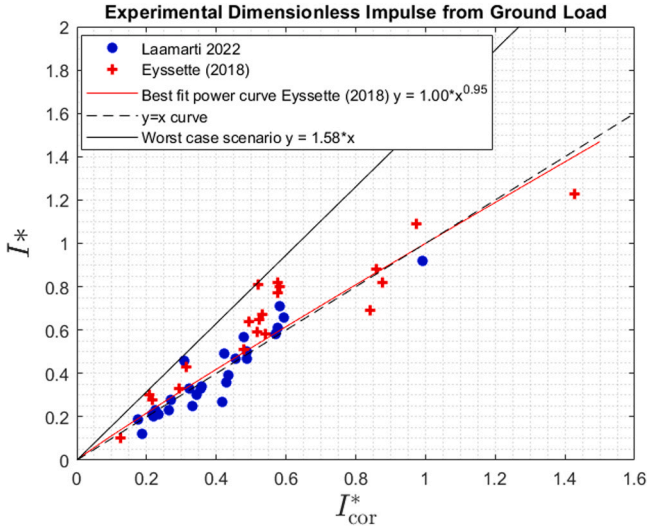

Fig. 11. Dimensionless Impulse.

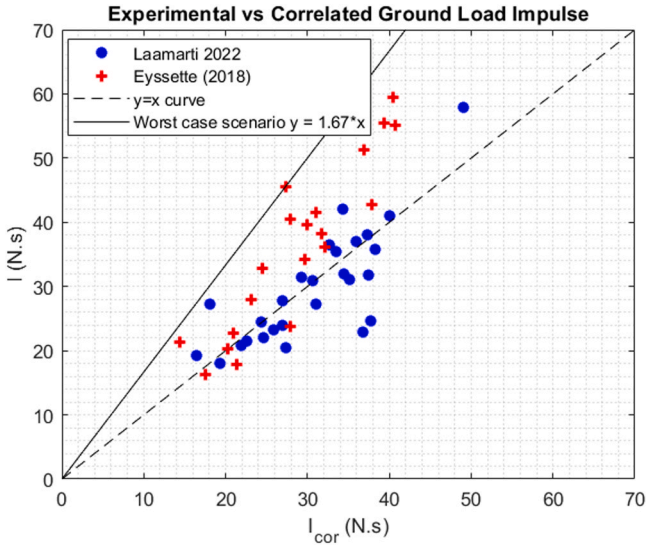

Fig. 12. Experimental vs Correlated Impulse.

6. Discussion and observations

6.1. Crack velocity

The crack velocity in a failing pressure vessel is related to the speed at which the vessel opens during failure. This dependent variable is considered one of the main factors behind the scatter seen in the data. We did not have any control over this variable. It would have been affected by the machining process we used to weaken the vessel. The opening speed of the vessel would depend on where the crack started. If the crack starts in the middle of the weakened length, then the vessel would open faster (cracks travel in both direction) than if the crack started at the end of the weakened length (crack travels in one direction). Controlling where the crack starts may reduce the scatter in the data.

Experiments have shown that strong shock overpressure and ground loading requires fast opening of the vessel. Other factors, such as large pressure vessel deflections, (flaps opening), details of the weakening of

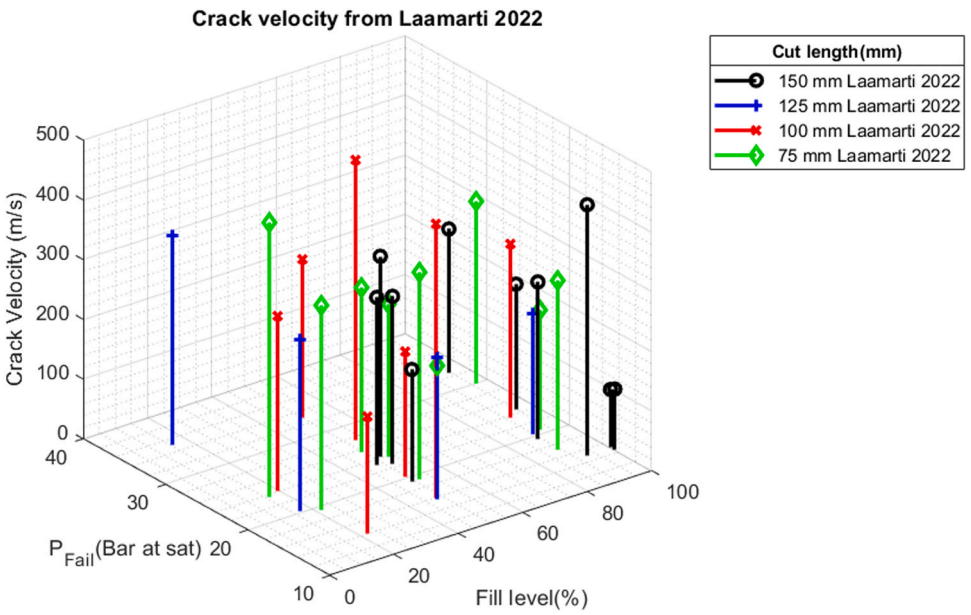

Fig. 13. Crack velocity BLEVE 2022.

Table 1
Vessel geometries of various scales, and ground loading estimation of a BLEVE (50% liquid fill level, P_f = 20 bar, L/D=6). The correlation has not been validated at larger scales and for different L/D.

BLEVE CASE		*Eyssette (2018)*	*Correlations*		*Worst case scenario*	
Reference	**Volume (m^3)**	**Peak Ground Force (kN)**	**Peak Ground Force (kN)**	**Impulse (kN.s)**	**Peak Ground Force (kN)** *(1.49*F_{cor})*	**Impulse (kN.s)** (1.67*I_{cor})
Small scale BLEVE	0.00054	25	22	0.029	33	0.048
(Birk and Cunningham, 1994)	0.403	1700	1726	27	2572	46
(Birk et al., 2006b)	1.9	6300	4803	109	7156	182
Johnson and Pritchard (1991)	5.7	14 400	10 176	341	15 161	571

the wall, and the transient pressure in the vessel will affect the crack speed. To gain a deeper understanding of the crack propagation behavior, researchers such as Emery et al. (1981) have investigated closely the phenomenon using the finite difference method. For cases where pressure vessel contains liquid, the rarefaction wave speed affected the crack speed ahead of the crack tip. All these cited complex interactions contribute to the overall failure mechanism of pressure vessels.

In the 2022 BLEVE experiments, high speed video was employed to measure the average crack speed. The values obtained are presented for informational purposes only. To ensure accuracy, further investigation using high-speed cameras is needed.

Fig. 13 shows the average crack speed based on high-speed video plotted with the independent variables of failure pressure, fill level, and weakened length. The graph shows the following trends.

i) Higher crack speed with higher failure pressure.
ii) Not sure what effect with fill level and weakened length.

Specifically, the failure pressure of the vessel has a direct relationship with the crack velocity; as this factor increase, the crack velocity tends to increase as well. But we do not control where the cracks start, and this affects the opening time. The highest crack speed was seen at the 50% liquid full. We also saw high crack speeds at 20 and 90% but low crack speed at 100% fill. The trend with fill is not clear. Further work is needed to control the crack speed in the testing. Future tests will include machining that causes the crack to start in the center of the weakened length.

6.2. *Application of correlations to larger case scenarios*

The developed correlations for ground load apply only to the small

scale as tested (D= 50 mm, L= 300 mm,L_v/D =6). The question is – can this be used for larger scales? It is important to note that these correlations have not undergone validation for larger scale scenarios as of now. Assuming that these correlations can be scaled, the ground load has been estimated for other cases. The following examples are presented:

- Birk and Cunningham (1994): The vessel is 0.4 m^3 approximately 684 times larger in mass and volume compared to BLEVE 2022. The vessel specifications are as follows:
  - V = 0.403 m^3 / L=1.52 m /D=0.61 m
- Birk et al. (2006): The vessel is 1.8 m^3 about 3325 times larger than BLEVE 2022. The vessel specifications are as follows:
  - V = 1.9 m^3 / L=3.07 m / D=0.953 m /L_c= 2.12 m
- Johnson and Pritchard (1991): The vessel is 5.7 m^3 approximately 9677 times larger in mass and volume compared to BLEVE 2022. The vessel specifications are as follows:
  - V = 5.7 m^3 / L=5 m / D=1.2 m /L_c= 3.8 m

  Similar initial conditions of rupture were applied on the above cases and are presented as follow:
  - P_f= 20 bar - 50% liquid fill level.

Eyssette (2018) tried to upscale the maximum peak force with the opened area of the failing vessel. Subsequently, this approach will be compared to the derived correlations.

Table 1 demonstrates that upscaling the peak ground force falls within the bounds defined by the average correlation values and the most adverse case scenario. The results imply that the magnitudes of forces and impulses can be very substantial when dealing with full-scale tanks. It is important to reiterate to the reader that these predictions lack validation and should be used with great caution.

7. Conclusion

The small-scale BLEVE experiments provided a unique opportunity to investigate ground loading from BLEVE using state of art data acquisition technologies. A predictive correlation has been developed that has inputs of vessel size, burst pressure, fill level, and weakened length. The correlation outputs are peak ground force, force duration and impulse. The analysis of these parameters revealed significant influence of the liquid phase in increasing both the ground load force and its duration. BLEVE incidents with the vessel close to 95% full of liquid exhibited the highest ground loads. However, cases with 100% fill level showed a completely different behavior, by exhibiting the lowest peak ground load, Although the correlations did not include the 100% fill level cases, it is noteworthy that their peak ground load consistently registers significantly below the correlation established for peak ground load.

The methodology comprises semi-empirical approaches designed to yield simple correlations, which serve the purpose of evaluating BLEVE ground loads. Prediction models are introduced as initial approximations for determining the maximum ground load, the duration of ground load and impulse. Extrapolation of the correlations to larger dimensions provides a quantitative understanding of the magnitude involved in such incidents. Their current applicability lies in offering estimations of the potential forces rather than serving as definitive tools for comprehensive safety assessments. Further work is necessary to validate the correlations for larger scales.

Declaration of Competing Interest

The authors declare the following financial interests/personal relationships which may be considered as potential competing interests. El Mehdi Laamarti reports financial support was provided by Queen's University and IMT mines Ales. If there are other authors, they declare that they have no known competing financial interests or personal relationships that could have appeared to influence the work reported in this paper.

Appendices

Summary table of BLEVE operating conditions

The fill levels illustrated in the following figure are approximations, influenced by factors such as leaking and measurement imprecision. Nevertheless, instances with 100% fill levels are conclusively confirmed by steep pressure rise obtained from the pressure trace, indicating the transition of the liquid into a compressed state.

Table 1
BLEVE Operating conditions

Laamarti 2022				Eyssette (2018)			
Test	Lc(mm)	Pfail(barg)	Fill (%)	Test	Lc(mm)	Pfail(bara)	Fill (%)
1	150	19.8	100	2	150	11.7	52
2	150	24.0	95< φ <100	3	150	13.4	55
3	150	no data	no data	4	150	15.6	59
4	150	31.7	95< φ <100	5	150	16.7	63
5	150	no data	no data	6	150	17.0	59
6	150	23.1	51.7	7	100	18.8	58
7	150	18.6	49.4	8	100	12.5	57
8	150	22.6	48.3	9	50	19.0	55
9	150	21.9	51.8	10	50	19.1	15
10	150	14.2	92.7	11	150	17.7	17
11	150	13.8	100	12	150	19.1	95< φ <100
12	150	24.9	100	13	150	15.8	95
13	150	no data	no data	14	150	18.3	18
14	150	no data	no data	15	150	15.5	Air
15	150	19.0	89.0	16	150	16.0	5
16	150	34.0	15.3	17	150	21.2	100
17	100	14.9	47.8	18	150	18.5	61
18	100	23.2	91.1	19	150	30.6	65

(continued on next page)

Table 1 (*continued*)

Laamarti 2022				Eyssette (2018)			
19	100	27.2	52.5	20	150	26.9	63
20	100	23.2	19.4	21	150	19.3	85
21	75	18.6	21.3	22	150	23.3	87
22	75	14.9	48.2	23	150	32.7	70
23	75	17.0	88.9	24	150	26.3	24
24	75	23.1	53.6	25	150	29.5	18
25	100	13.9	22.2	26	75	18.6	57
26	100	19.5	49.7				
27	100	20.7	92.5				
28	75	25.2	49.9				
29	75	23.5	16.0				
30	75	18.3	51.4				
31	75	29.4	96.3				
32	75	22.8	100				
33	125	19.3	16.8				
34	125	14.8	47.8				
35	125	19.7	89.3				
36	125	32.3	50.5				

Choked boiling wave model

The flashing phenomenon as the vessel opens is a complex 3D transient (unsteady) process. This process leads to the rapid (in milli-seconds) emptying of the pressure vessel over time. The actual process unfolds as a dynamic, non-equilibrium, nonhomogeneous, and three-dimensional transient event. For our correlation, we wanted to estimate an approximate time for the liquid release assuming a simple 1D boiling wave. We assume a constant mass flow rate for the duration of the release. For the analysis, certain simplifying assumptions have been adopted:

- 1D boiling wave.
- Boiling wave moves downward into stationary liquid (unsteady)
- Move with the boiling wave to make it a quasi-steady-state condition (liquid moves up relative to stationary boiling front, 2-phase flow moves up after pressure drop)
- Assuming thermodynamic equilibrium between phases
- Homogeneous equilibrium of 2-phase mixture (same T, P and velocity).
- Assume pressure drop at boiling front that gives choked 2 phase-flow.
- Pressure drop is isentropic (adiabatic, reversible)
- Accounting for the energy associated with the phase change.
- Neglecting work done, elevation changes, heat transfer, and losses (isentropic process)
- Assuming constant pressure and temperature in the liquid.
- Pure propane

The calculation gives us a velocity and mass flux of the two-phase mixture above the boiling wave. We use this to represent the 2-phase release.

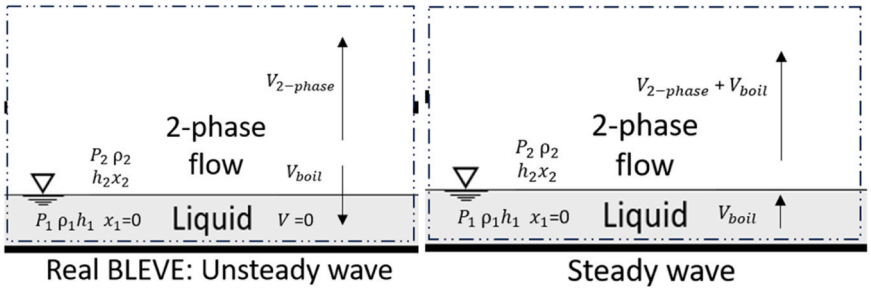

Fig. 1. Boiling wave in unsteady and steady coordinates.

We move with the boiling wave to make the problem steady as illustrated in Fig. 1.

The three fundamental conservation laws of thermodynamic namely mass, momentum, energy can be formulated and applied across the entire control volume.

$$\dot{m} = \rho_1 A V_{boil} = \rho_{2-phase} A \quad (V_{boil} + V_{2-phase}) \quad A = constant$$

$$H_0 = h_1 + \frac{V_{boil}^2}{2} = h_{2-phase} + \frac{(V_{boil} + V_{2-phase})^2}{2}$$

$$(P_1 - P_{2-phase})A = \dot{m}(V_{boil} + V_{2-phase} - V_{boil})$$

$$\dot{m}_{unsteady} = \rho_{2-phase} \quad V_{2-phase} \quad \text{Ratio} = \frac{P_{2-\text{phase}}}{P_1} \tag{7}$$

$\dot{m}$: steady mass flow rate [kg/s]
A: Surface of the pressure vessel [m^2]
$\dot{m}_{unsteady}$: mass flow rate [kg/s]
V_{boil} : Boiling wave velocity [m/s]
$V_{2-phase}$: 2-phase flow velocity [m/s]
ρ_1: Density at state 1 [kg/ m^3]
$\rho_{2-\text{phase}}$: Density at state 2 [kg/ m^3]
H_0: Total enthalpy [J/kg]
h_1: Enthalpy at state 1 [J/kg]
$h_{2-\text{phase}}$: Enthalpy of 2-phase [J/kg]
P_1: Saturation pressure at state 1 [Pa]
x_1: quality of state 1
$P_{2-\text{phase}}$: Pressure at state 2 [Pa]

By assuming an isentropic process, the momentum equation is not needed which results in a system of two equations with two unknowns. The flow is choked at the vessel opening area. The determination of choked flow conditions is done by finding the maximum transient mass flow rate across various pressure ratios. The model presented herein was solved using Engineering Equation Solver (EES) by F-Chart Software, enabling the prediction of both boiling wave speed and the time required for complete vessel emptying.

Fig. 2 illustrates the boiling wave mass flux rate for different failure pressures, while Fig. 3 showcases the boiling wave speed under various failure pressure conditions. Notably, the boiling wave model aligns well with experimental findings. Experimentally, through high-speed videos and post-treatment images, the boiling wave velocity, captured from a side view, can be determined. However, it should be acknowledged that the model tends to slightly overestimate the ground load duration compared to experimental outcomes due to irreversibility in real-life scenarios. Nevertheless, the model delivers consistent and conservative results.

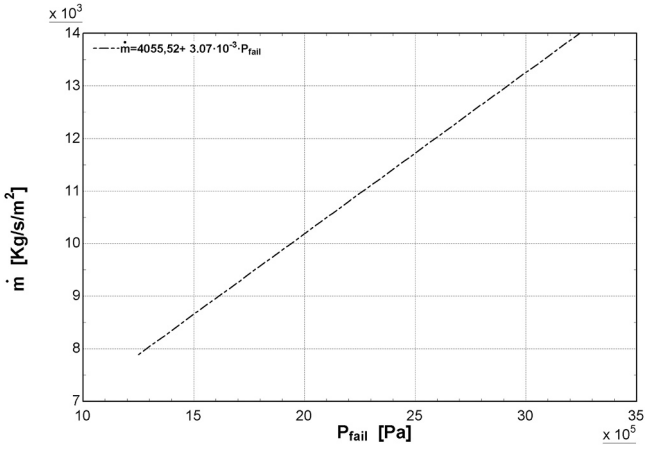

Fig. 2. Boiling wave mass flux rate.

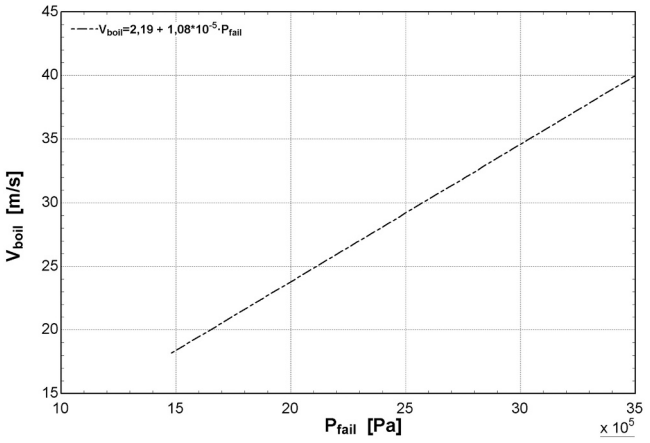

Fig. 3. Boiling wave speed

Compressible vapor model

Throughout the duration of vapor release, the assumption of choked vapor flow emanating through the opening of the vessel is adopted. The compressible flow model derived from the momentum conservation equation is used to predict the expansion speed of the vapor phase during the BLEVE.

$$\dot{m}_{vap} = \rho_2 V_2 A = \rho_2 V_{vap} A \quad (8)$$

$\dot{m}_{vap}$: Steady mass flow rate of vapor [kg/s]
A: Surface of the pressure vessel [m^2]
V_2: Volume at state 2 [m^3]
ρ_2: Density at state 2 [kg/ m^3]
V_{vap} : Velocity of vapor phase [m/s]The presented model was solved using EES by F-Chart Software and the corresponding results are presented through the following curves:

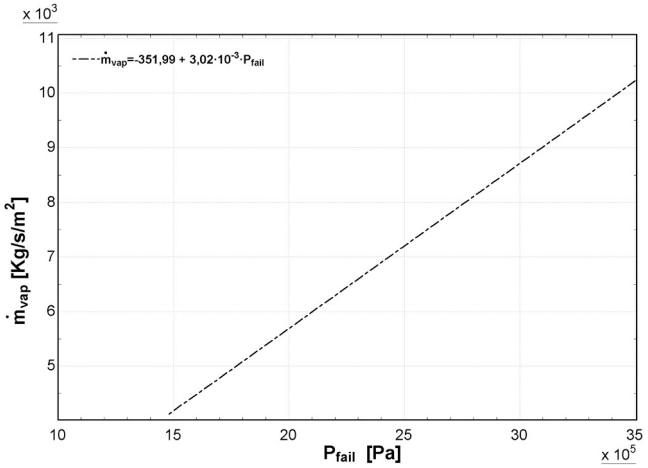

Fig. 4. Vapor mass flux rate

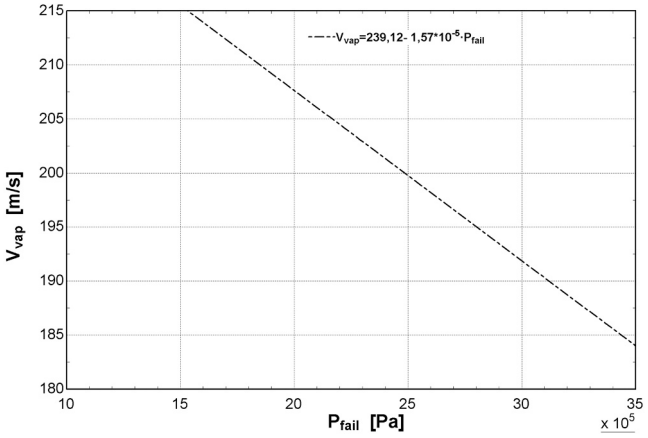

Fig. 5. Vapor speed

By referring to Figs. 4 and 5, the vapor wave speed and the steady mass flow rate can be determined based on the failure pressure. Unlike the boiling wave speed, the vapor wave speed demonstrates a decreasing trend as the failure pressure varies.

Duration of ground load equations

From the first law of mass conservation:

$$\dot{m}_1 = \rho_1 V A_1$$

$$\dot{m}_{liq} = \rho_{liq} V_{boil} A_{liq\_surf}$$

$$t_{liq} = \frac{m_{liq}}{\rho_{liq} V_{boil} A_{liq\_surf}}$$

Similarly, to the liquid phase, the vapor phase can be written as follow:

$$t_{vap} = \frac{m_{vap}}{\rho_{vap} V_{vap} A_{liq\_surf}}$$

Where,

$$m_{vap} = \rho_{vap}(1-\varphi)V$$

$$A_{liq\_surf} = L_c D$$

$$V = L_v * \pi * \frac{D^2}{4}$$

$$m_{liq} = \rho_{liq} \varphi V$$

$$\varphi = \frac{\frac{m_{liq}}{V} - \rho_{vap}}{\rho_{liq} - \rho_{vap}}$$

D : Diameter of the vessel [m]
t_{liq} : Calculated duration of liquid phase [s]
t_{vap} : Calculated duration of vapor phase [s]
V_{vap} : Calculated velocity of the vapor phase [m/s]
V_{boil} : Calculated boiling wave velocity [m/s]
m_{vap} : Mass of the vapor phase [kg]
ρ_{liq}: Density of the liquid phase [kg/ m^3]
ρ_{vap}: Density of the vapor phase [kg/ m^3]
V: Pressure Vessel volume [m^3]
φ: Liquid fill level [%]
A_{liq_surf}: Area of Liquid surface [m^2]
m_{liq} : Mass of the liquid phase [kg]

References

Abbasi, T., Abbasi, S.A., 2007. The boiling liquid expanding vapour explosion (BLEVE): mechanism, consequence assessment, management. J. Hazard. Mater. 141, 489–519.

BBC news (6 August 2018) Bologna crash: Tanker truck fireball kills two and injures dozens ref: www.bbc.com/news/world-europe-45087884.

Birk, A., Davison, C., Cunningham, M., 2007. Blast overpressures from medium scale BLEVE tests. J. Loss Prev. Process Ind. 11/View Content/3612385/View.

Birk, A.M., 1996. Hazards from propane BLEVEs: an update and proposal for emergency responders. J. Loss Prev. Process Ind. 9 (2), 173–181. https://doi.org/10.1016/0950-4230(95)00046-1.

Birk, A.M., Cunningham, M.H., 1994. The boiling liquid expanding vapour explosion. J. Loss Prev. Process Ind. 7, 474–480.

Birk, A.M., Poirier, D., Davison, C., 2006. On the response of 500 gal propane tanks to a 25% engulfing fire. J. Loss Prev. Process Ind. 19, 527–541. https://doi.org/10.1016/j.jlp.2005.12.008.

Birk, A.M., Eyssette, R., Heymes, F., 2019. Early moments of BLEVE: from vessel opening to liquid flashing release. Process Saf. Environ. Prot. 132, 35–46 doi: 10.1016/j.psep.2019.09.028. [hal-02428264].

Birk, A.M., Heymes, F., Eyssette, R., Lauret, P., Aprin, L., Slangen, P., 2018. Near-field BLEVE overpressure effects: the shock start model. Process Saf. Environ. Prot., S0957582018301101 https://doi.org/10.1016/j.psep.2018.04.003.

CTV news South Africa gas truck explosion death toll rises to 34 ref: https://www.ctvnews.ca/world/south-africa-gas-truck-explosion-death-toll-rises-to-34-1.6214884 (24th December 2022).

Emery, A.F., Kobayashi, A.S., Love, W.J., "Dynamic crack propagation in pipes" (1981), Department of Mechanical Engineering, University of Washington, Seattle, Washington 98195.

Eyssette, R., 2018. Characterization and modeling of near-field BLEVE overpressure and ground loading hazards. Queen's University (Canada) / IMT Mines Ales (France).

Eyssette, R., Heymes, F., Birk, A.M., 2021. Ground loading from BLEVE through small scale experiments: experiments and results. Process Saf. Environ. Prot. 148, 1098–1109. https://doi.org/10.1016/j.psep.2021.02.031.

Johnson, D.M., Pritchard, M.J., 1991. A large-scale experimental study of BLEVEs. British Gas Report No I536, United Kingdom..

Laboureur, D., Birk, A.M., Buchlin, J.M., Rambaud, P., Aprin, L., Heymes, F., Osmont, A., 2015. A closer look at BLEVE overpressure. Process Saf. Environ. Prot. 95, 159–171.

Laboureur, Delphine; Buchlin, Jean-Marie; Rambaud, Patrick (2012). [ASME ASME 2012 Pressure Vessels and Piping Conference - Toronto, Ontario, Canada (Sunday 15 July 2012)] Volume 9: Rudy Scavuzzo Student Paper Symposium and Competition - Small Scale Experiments on Boiling Liquid Expanding Vapor Explosions: Supercritical BLEVE., 51–. doi:10.1115/PVP2012-78283.

Planas-Cuchi, E., Salla, J.M., Casal, J., 2004. Calculating overpressure from BLEVE explosions. J. Loss Prev. Process Ind. 17, 431–436.